AALBORG UNIVERSITY
STUDENT REPORT

CFD simulation of H_2S Scavenger injection

PECT 10 - Master's Thesis

Aalborg University, Campus Esbjerg
Niels Bohrs Vej 8
6700 Esbjerg

May 30, 2019

Title page

Subject : H2S Scavenger
Project title : CFD simulation of H_2S Scavenger injection
Project group : PECT10-5-F19.
Semester : 10th semester.
ECTS : 30
Supervisor : Matthias Mandø
Faculty : Aalborg University, Campus Esbjerg.

Author

Emil Tornel Jørgensen

Abstract

When treating the sour gas, excessive use of scavenger is often seen because of the use of a quill as an injection. The purpose of this study is an investigation of the survival of the scavenger in the pipeline by nozzle injection. The scavenger requires a sufficient time to react with the gas and is therefore relevant due to particle survival. The primary part of this study is a CFD simulation of the H_2S injection with a nozzle. Different injection direction is investigated to check the effectiveness of that. Furthermore, a change in the pipe design is investigated to see whether this has an influence on the particle survival.
The simulations showed that the large particles was not able to be carried from the flow, and therefore falls to the bottom of the pipe. While the small particles survives and got sufficient time to react with the H_2S.

Reading Guide

To distinguish between figures, equations, and citations, [] is used for referring to citations and numbers used for referring to figures and equations.

Preface

In table 1 constants used throughout the study, is listed. The table contains specifications from the gas phase and the injection product, as well as specifications of the geometries.

Table 1: Table of the used constants

Density of the continuous phase	ρ_c	$11.8 \left[\frac{kg}{m^3}\right]$
Density of the particles	ρ_p	$1200 \left[\frac{kg}{m^3}\right]$
Viscosity of the continuous phase	μ_c	$1.249 \cdot 10^{-5} \left[\frac{kg}{ms}\right]$
Viscosity of the particles	μ_p	$6.34 \cdot 10^{-3} \left[\frac{kg}{ms}\right]$
Velocity of the continuous phase	u	$10 \left[\frac{m}{s}\right]$, $20 \left[\frac{m}{s}\right]$, $40 \left[\frac{m}{s}\right]$
Velocity of the discrete phase	v	$1.234 \left[\frac{m}{s}\right]$
Diameter of the pipe	D	10 cm
Length of the pipe	L	1000 cm
Particle diameter	d_p	Particle distribution

Contents

Chapter 1

Background of H_2S Scavenger Injection

Crude oil is a naturally occurring process from organic material. Through the oil formation, the organic material release gases which can contain toxic gases such as hydrogen sulfide (H_2S). H_2S is a colorless gas with the characteristic odor of rotten eggs and is extremely dangerous for humans and corrosive to metals. Therefore, treatment of this gas is necessary before transferring it ashore. Usually, a quill is used for the injection of the scavenger. Figure 1.1 is an illustration of the quill in the pipeline. The quill works thus, it pours the chemical into the gas stream.

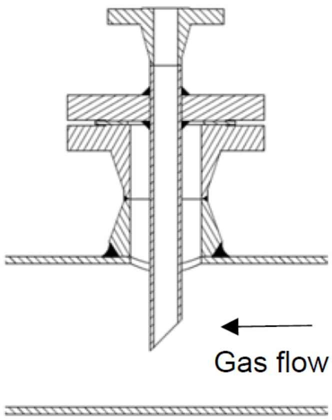

Figure 1.1: Illustration of a quill installation [1]

Excessive use of chemicals is often seen, and the efficiency of the process is very poor. Stoichiometry calculations could estimate the right amount of scavenger, but usually, 2-5 times more scavenger is used [2].

1.1 Analysis

This chapter is an analytical study of the injection system and the parameters behind it. The study contains an explanation of the injection system, the hydrogen sulfide gas and the risks behind it, and the different scavenger which can be used in the treatment process.

1.1.1 Direct Injection System

On the offshore field, space and weight are a limiter for installation of scavenger systems. Therefore, direct injection systems, as illustrated in figure 1.2, are the most commonly used at offshore applications. The scavenger is sprayed directly into the gas stream. Direct injection is excellent where there is sufficient time to react with the H_2S. Suppliers recommend a minimum of reaction time on 15-20 seconds [3].

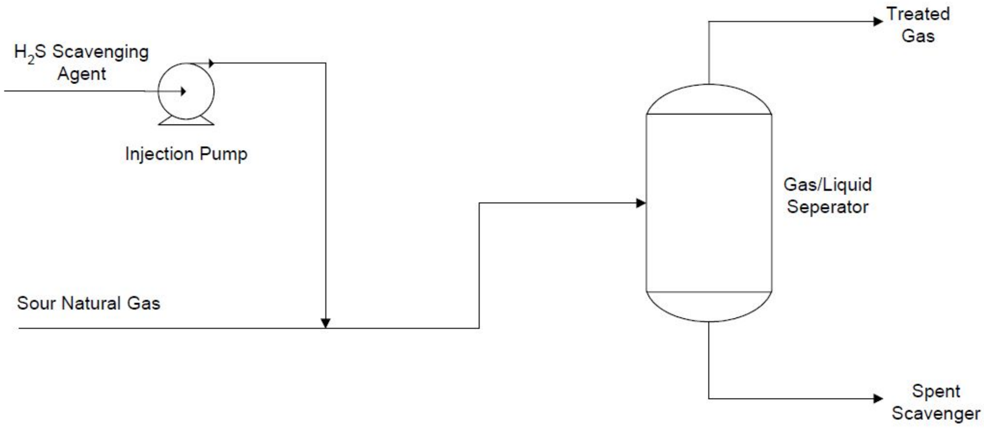

Figure 1.2: Illustration of a typical direct injection system [1]

The typical system consists of an injection pump, injection directly into the pipeline, a given length of the pipe (For the reaction between scavenger and H_2s) and a scrubber. The injection pump is pumping the chemical into the pipeline. The direct injection is through a quill, injection mixer, or nozzle atomizer. It is assumed that a nozzle atomizer will deliver a better survival of the particle and is therefore used in this study. A gas-liquid separator uses gravity to separate the mixture. The spent or excess scavenger agent falls to the bottom, and the treated gas rises to the top.

Figure 1.3 is a illustration of the injection types.

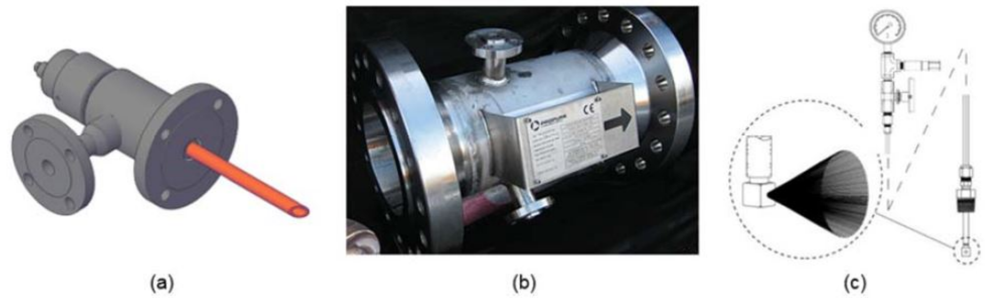

Figure 1.3: (a) Injection quill, (b) Injection mixer, (c) Atomizing nozzle [1]

The injection mixer is also known as an inline mixer. An injection mixer is used to mix two or more fluids. The injection mixer is illustrated in figure 1.4, and is very useful to make a homogeneous mass.

Figure 1.4: Illustration of an injection mixer inside [4]

Hydrogen sulfide (H_2S) is a gas found in the drilling and production of crude oil. H_2S is a gas which is naturally released in the microbial breakdown of organic material. As previously mentioned, it is extremely toxic for humans, even at small concentrations. People smell it at low concentrations, as table 1.1 illustrates, only 50% of humans detect H_2S at a concentration on 0.0047 ppm, and at high concentration, people lose their ability to smell it. H_2S is flammable and highly corrosive to steel, which is crucial for pipes and valves [5].

Table 1.1: Table of the effects at different concentrations of H_2S [6]

Concentration and Effects of H_2S	
0.0047 ppm	The concentration where 50% of humans can detect the characteristic odour of H_2S
10-20 ppm	Is the limit concentration for eye irritation
50-100 ppm	Leads to eye damage
150-250 ppm	The smell nerve is paralysed after a few inhalations, and the sense of smell disappears, often together with awareness of danger
320-530 ppm	Leads to water in the lungs with the possibility of death
530-1000 ppm	Causes strong stimulation of the central nervous system and rapid breathing, leading to loss of breathing.
over 1000 ppm	Inhalation of a single breath, causes immediately collapse with loss of breathing

People working in the north sea, where there are operations of petroleum and natural gas drilling, can be exposed to larger amounts of H_2S than in the general population. Typically the natural gas contains 0-200 ppm, but in some cases, the concentration is at 500-3500 ppm. In Kazakhstan has there been a case with a concentration on 20.000 ppm [7].

1.1.2 Scavengers

H_2S scavenging, also known as gas sweetening process, is a critical and economic aspect to ensure safety for humans, and for ensuring trouble-free upstream and downstream operations. There are two different kinds of scavengers: solid scavengers and liquid scavengers. Various aspect has significant on the optimal strategy, such as operational expenditure (OPEX) and capital expenditure (CAPEX) as well as space and weight.

Solid Scavengers

The usefulness of solid scavengers are quite good, they are very effective in removing H_2S and are predictable in their removing rate. Although solid scavengers require low OPEX, they require significant CAPEX. The used scavenger of the non-regenerative solid requires removal or disposal, which makes it impractical for offshore applications. Another significant impact that makes it less practical for offshore use is that solid scavengers require further installations.

Liquid Scavengers

Liquid scavengers are useful for offshore applications, where space and weight are a significant parameter, they require less weight and space than solid scavengers. But liquid scavengers are generally less efficient, and OPEX is significantly higher. An important feature, which makes it ideal for offshore applications is that liquid scavengers offer more option for retrofitting an existing facility. Liquid scavengers fall into two categories: Regenerative- and Non-Regenerative Scavengers, as illustrated in table 1.2.

Table 1.2: Table of the Regenerative- and Non-Regenerative Scavengers [3]

Regenerative Scavengers	Non-Regenerative Scavengers
Amine Wash	Aldehydes
Reduction Oxidation	Triazine
	Sodium Nitrate

Triazine is the most commonly used in the offshore industry and is the one used in this project. The by-product of the reaction is soluble in the oil or water phase, but unreacted triazine is highly toxic for aquatic life, therefore, over-treatment of the gas should be minimized [8].

Chapter 2

Previous Work

Based on the background of the H_2S scavenger injection, the previous study is investigated. Examination of the optimum design is made: The Gas Technology Institute (GTI) has made a study of multi-pipe direct injection [9]. While other studies have focused on different injection methods and design rules [1]. In the optimum design work, pipe dimensions, the location of a mixer and design principles are important parameters.

The performance of injection systems is challenging to predict because the diameter and the length of the pipe have an influence on the reaction. Study of the optimum dose rate by mathematically modeling and simulation validation is made [10]. Furthermore, a study of the optimum injection dose concluded that the pipe diameter, pipe length, gas flow rate, pressure, and temperature had an influence in the injection dose rate [11][12].

There are two different kind of scavengers: Regenerative- and non-Regenerative scavengers. The efficiency of commercial scavengers is investigated and showed different efficiencies in the ability to capture H_2S in the gas [13]. Another thing that is investigated in the scavenger section is the ratio between the scavenger and the gas [14].

.

The previous study of H_2S scavenger provides access to the project definition.

2.1 Project Definition

Based on the literature study and the analysis study, the project definition can be stated. The amount of scavenger injection is not defined, and usually, the injection dose rate is determined by experimental lab tests and field trials. Typical efficiency is approximately 40% removal of H_2S, but injection location and product selection must be carefully considered to be effective [3]. The previous work showed that the pipe diameter, pipe length, gas flow rate, pressure, and temperature had an influence on the efficiency on the scavenging process. Therefore, the reaction between H_2S and scavenger is a relevant topic.
No study showed the optimum direction of the injection in the pipe, therefore, the direction of the injection could have an impact on the efficiency when removing H_2S. As mentioned previously a quill is usually used for the injection, the quill pours the scavenger into the gas stream. Based on the low efficiency of the removal, the quill is assumed as poor. Therefore, this project will be stated on nozzle atomizing of the H_2S injection, which is assumed to be better for the process, and will be answering the following:

What is the impact of the nozzle on the particle survival?

What is the optimum injection direction of the nozzle?

What is the optimum particle size for the system?

What is the impact on particle survival, by a change in the design of geometry?

To answer these questions, a theoretical study of the scavenger is made, along with a CFD simulation to examinees the physical problem with computational power.

Chapter 3

CFD Simulation

This chapter will contain an explanation of the simulation in this project. First, the governing equation behind the simulation is investigated and listed. Then the meshing section is reviewed to investigate the quality of the created mesh. Furthermore, particle-fluid interaction is explained to review the flow. At the end of this chapter, a simulation explained with the set-up, simulations, and results.

3.1 Computational Fluid Dynamics

Computational Fluid Dynamic (CFD) is an analyzing tool for engineering problems in fluid mechanics. CFD is structured around a numerical algorithm and is the ideal tool for solving fluid flow problems. [15]
Many different software's are available according to mathematical models, numerical methods, computational equipment, and post-treatment. For this project, cubit software is used for the pre-processing, and Ansys Fluent is used for the simulation and post-treatment.

3.2 Governing Equations

For solving the fluid flow, Ansys Fluent solve a set of equation. For the continuous flow, the continuity- and momentum equation is solved. For the prediction of the particle motion, a set ordinary differential equations are solved. This section will include an explanation of the underlying equations.

3.2.1 Conservation Of Mass

For the continuous phase, the conservation of mass in a closed system is described by the continuity equation. Since the continuous phase is an incompressible flow the continuity equation is stated as:

$$\frac{\partial u_i}{\partial x_i} = 0 \tag{3.1}$$

Where:

- u = The velocity of the continuous phase

3.2.2 Reynolds-Averaged Navier-Stokes

The RANS equation is solved in the simulation, and are the time-averaged equations for the fluid flow. The RANS are often used in turbulence flow, to account for the fluctuating quantities. RANS equation is stated in equation 3.2:

$$\frac{\partial \bar{u}_i \bar{u}_j}{\partial x_j} = -\frac{\partial \bar{P}}{\partial x_i} + \frac{\partial}{\partial x_j}\mu_t \left(\frac{\partial \bar{u}_i}{\partial x_j} + \frac{\partial \bar{u}_j}{\partial x_i}\right) + g_i + S_p \tag{3.2}$$

Where

- ρ = The density of the continuous phase
- $\bar{P}$ = The average pressure
- μ_t = The turbulent viscosity

3.2.3 Turbulence Model

To account for the turbulent flow, the standard k-ϵ is used and is based on model transport equation. The (k) accounts for the kinetic energy while the (ϵ) accounts for the dissipation rate.
The k-equation:

$$\frac{\partial}{\partial t}(k) + \frac{\partial}{\partial x_j}(k\bar{u}_j) = \mu_T \left(\frac{\partial \bar{u}_i}{\partial x_j} + \frac{\partial \bar{u}_j}{\partial x_i}\right)\frac{\partial \bar{u}_i}{\partial x_j} + \frac{\partial}{\partial x_j}\left(\mu + \frac{\mu_T}{\sigma_k}\frac{\partial k}{\partial x_j}\right) - \epsilon \tag{3.3}$$

While the ϵ equation is as following:

$$\frac{\partial \epsilon}{\partial t} + \frac{\partial \bar{u}_j \epsilon}{\partial x_j} = \frac{\partial}{\partial x_j}\left(\mu + \frac{\mu_T}{\sigma_\epsilon}\frac{\partial \epsilon}{\partial x_j}\right) + C_{\epsilon 1}\frac{\epsilon}{k}\mu_t \left(\frac{\partial \bar{u}_i}{\partial x_j} + \frac{\partial \bar{u}_j}{\partial x_i}\right)\frac{\partial \bar{u}_i}{\partial x_j} - C_{\epsilon 2}\frac{\epsilon}{k}\epsilon \tag{3.4}$$

The turbulent viscosity is expressed as:

$$\mu_t = C_\mu \rho \frac{k^2}{\epsilon} \tag{3.5}$$

Where $C_{\epsilon 1}$, $C_{\epsilon 2}$ and C_μ are constant. σ_k and σ_ϵ are the turbulent Prandtl numbers for k and ϵ:

- $\sigma_k = 1.0$
- $\sigma_\epsilon = 1.3$
- $C_{\epsilon 1} = 1{,}44$
- $C_{\epsilon 2} = 1{,}92$
- $C_\mu = 0.09$

3.2.4 Particle Motion

The particle motion is determined by a set of ordinary differential equations (ODE's). The trajectory of the particle is predicted by integrating the force balance on the particle. The particle force balance is stated as:

$$\frac{d\vec{u}_p}{dt} = \frac{\vec{u} - \vec{u}_p}{\tau_r} + \frac{\vec{g}(\rho_p - \rho)}{\rho_p} \tag{3.6}$$

Where:

- $\dfrac{\vec{u} - \vec{u}_p}{\tau_r}$ = The drag force per unit particle mass

τ_r is the particle relaxation time and is expressed as:

$$\tau_r = \frac{\rho_p d_p^2}{18\mu} \frac{24}{C_d Re} \tag{3.7}$$

Where:

- $\vec{u}$ = Fluid phase velocity
- $\vec{u_p}$ = Particle velocity
- μ = Viscosity of the fluid
- ρ = Fluid density
- ρ_p = Particle density
- d_p = Particle diameter
- C_d = Drag coefficient

The drag coefficient is calculated by:

$$C_D = 24/Re \tag{3.8}$$

The Reynolds number is presented by:

$$Re = \frac{\rho d_p |\vec{u_p} - u|}{\mu} \tag{3.9}$$

3.3 Meshing

This section will explain the geometries and the meshing part of them. Furthermore, a study of the mesh is investigated later on.

3.3.1 Geometry

For this study, two geometries are used, to see if one of them will affect the effectiveness of the scavenging. The two geometries are illustrated in figure 3.1 and 3.2.

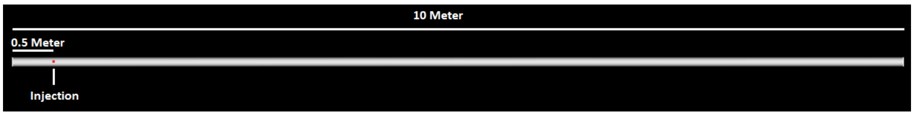

Figure 3.1: Illustration of the straight pipe geometry

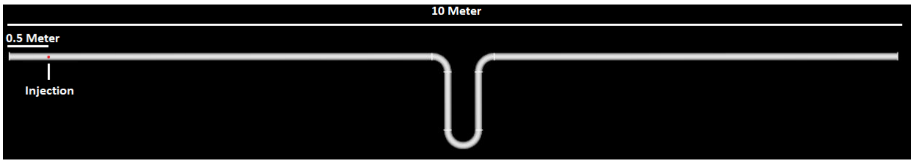

Figure 3.2: Illustration of the geometry with an U-bend

Figure 3.1 is a straight pipe, and figure 3.2 is a pipe with a u-bend, to see if this will affect the process positive or negative.

3.3.2 Mesh

To create the mesh, the Cubit software is used. Cubit software is a simple tool for creating two- and three-dimensional finite element meshes. It is based around a solid-modeler pre-processor, to create meshes of the volumes and surfaces for finite element analysis [16].

The mesh created on both of the geometries is a full hex mesh. The meshes are created by pave mesh and sweep algorithm. The pave is created on the end surface as illustrated in figure 3.3

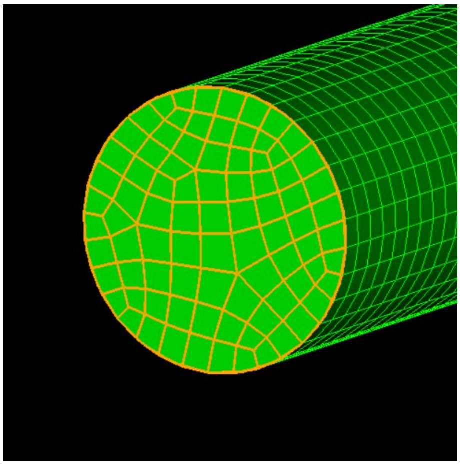

Figure 3.3: Illustration of the pave mesh

Pave mesh is used to mesh arbitrary three-dimensional surfaces and is an unstructured quadrilateral mesh. The sweep algorithm is used to produce an hex-mesh for the desired geometry. The algorithm is characterized by source and target surfaces. In this case, the source surfaces is meshed with the pave mesh, and then hex-mesh is extruded between the source and the target along a single-logical axis. The mesh near the wall is not refined because the focus is only on particle survival in this case.

3.4 Mesh Study

As previously mentioned, the mesh is studied, to check the quality. First of all, the right amount of cells need to be found. This is done in the grid independence study. Furthermore, the quality is defined by skewness and the aspect ratio of the cells. A good mesh is crucial for the accuracy and stability of the simulation.

3.4.1 Grid independence study

Grid independence study is important to see the right amount of cells to the mesh. Many cells are time-dependent and require a lot of computing power, which is why the smallest, but the right amount of cells is needed.

The study is made by simulating a simple flow and then see the change in pressure between the different amount of cells.

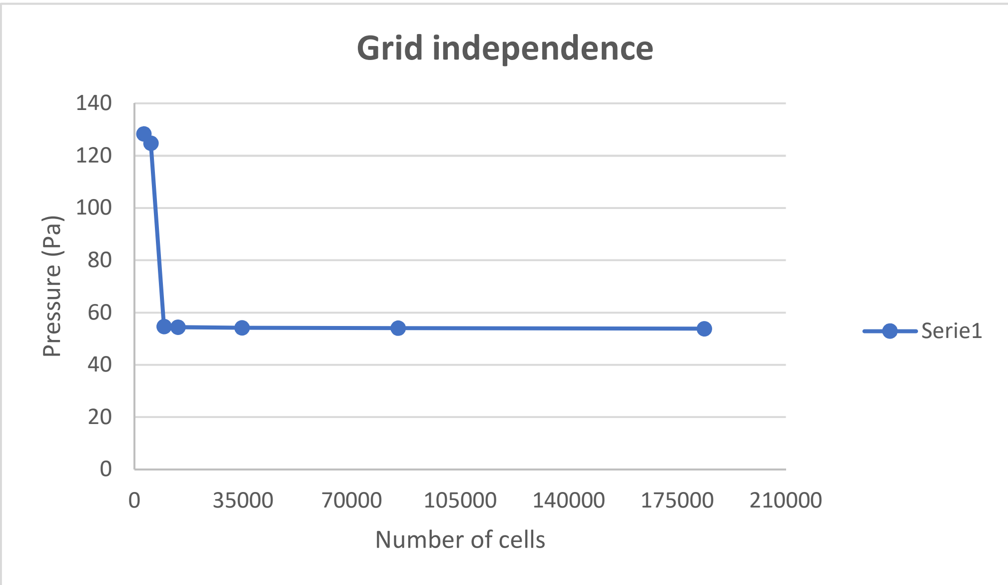

Figure 3.4: Graph of the grid independence study

Seven mesh resolutions were made: 3000 cells, 5350 cells, 9600 cells, 14000 cells, 34700 cells, 85000 cells, and 183.750 cells. By these results, the mesh with 9600 cells is the optimum mesh resolution due to computational power and still provide accurate results. Therefore the mesh with 9600 cells is used for further investigation.

3.4.2 Skewness

The skewness of the cells is a significant parameter for the simulation to converge. It is defined as, how close the cell is to an ideal cell, and if the skewness is to high the simulation will diverge instead of converging. The skewness is defined as:

$$Skewness = max\left[\frac{\theta_{max} - 90}{90}, \frac{90 - \theta_{min}}{90}\right] \tag{3.10}$$

Where:

- θ_{min} = The smallest angle in the cell
- θ_{max} = The largest angle in the cell

The values of the skewness are divided into different value to explain cell quality, and are listed in table 3.1:

Quality	Range
Perfect	0.00
Excellent	0.00-0.25
Good	0.25-0.50
Fair	0.50-0.75
Poor	0.75-0.90
Very poor	0.90-1.00
Degenerate	1.00

Table 3.1: Quality range of skew cells

If some of the cells are in the range of 'degenerate' or 'very poor' the simulation can have troubles with converging. Therefore, a new mesh may be necessary. The perfect mesh is having as many cells close to perfect.

Figure 3.1 is the investigation of the skewness in the mesh in the straight pipe.

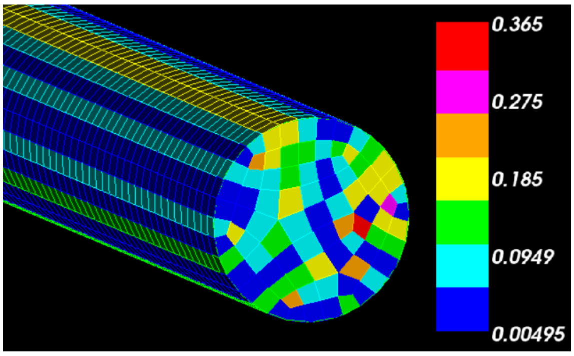

Figure 3.5: Skewness investigation of the straight pipe

As the figure illustrates the range of the cells are between 0.00495-0.365 and the mesh is of good quality and is seen as acceptable.

Figure 3.6 is the investigation of the skewness in the mesh of the U-pipe, and as the figure illustrates the mesh is also in the acceptable range.

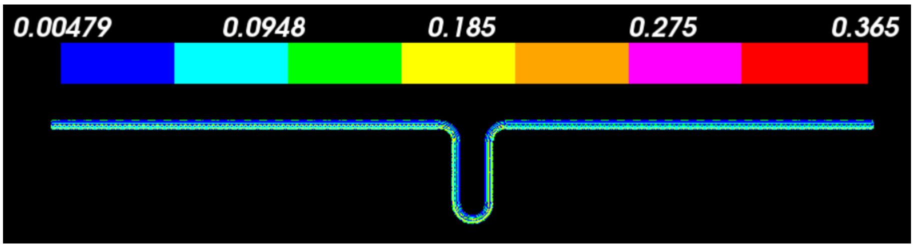

Figure 3.6: Skewness investigation of the U-pipe

The skewness of the meshes is acceptable and is not an issue for the simulation.

3.4.3 Aspect Ratio

Another thing to investigate is the aspect ratio, which is defined as the ratio between the longest and the shortest side in the cell. The aspect ratio indicates the perfection of the mesh and the perfect ratio between cells is 1. Figure 3.7 is the aspect ratio of the straight pipe, and is seen as acceptable.

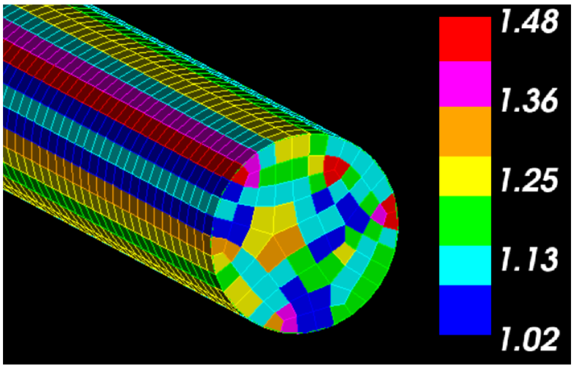

Figure 3.7: Aspect ratio investigation of the straight pipe

Figure 3.8 shows a bigger aspect ratio of the geometry with the U-bend. The ratios of the cells at the bend is a bit higher but is used for further study.

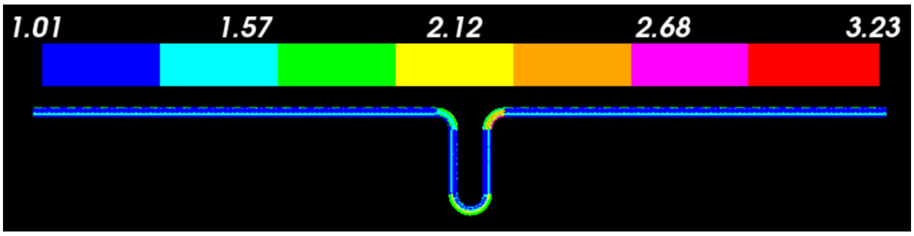

Figure 3.8: Aspect ratio investigation of the U-pipe

3.5 Simulation

3.5.1 Particle-Fluid Interaction

Dilute or Dense flow

This section is to check whether the motion of the particles is controlled by the continuous phase or not. A dilute flow is where the particle motion is controlled by the fluid forces. Dense flow is where the motion of the particles is controlled by collisions. Whether the dispersed flow is dilute or dense, is determined by the ratio of the momentum response time to the time between collisions.

$$\frac{T_V}{T_C} < 1 \qquad (3.11) \qquad\qquad \frac{T_V}{T_C} > 1 \qquad (3.12)$$

Equation 3.11 represent the dilute flow, where equation 3.12 represent the dense flow. T_V is the momentum response time. T_C is the average time between particle-particle collisions. Further explanation of the time ratio is in the appendix 6.1.
The dilute-dense plot shows the variation in the particle diameter with respect to the loading, which represents the dilute-dense regions:

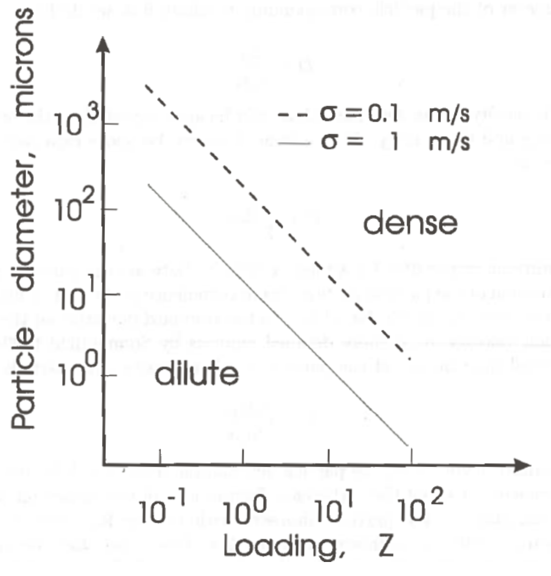

Figure 3.9: Dilute-Dense region plot [17]

The loading is expressed as the ratio between the mass flow rate of the dispersed phase and the mass flow rate of the continuous phase:

$$Z = \frac{\dot{M}_d}{\dot{M}_c} = \frac{0.003kg/s}{0.927kg/s} = 0.00324 \tag{3.13}$$

The calculation of the loading is in appendix 6.2.
The mean diameter of the particles is estimated as $38\mu m$ from figure 3.13, and the loading is calculated as 0.00324. Therefore, by looking at the graph, this study is in the dilute region.

Phase coupling

In multiphase flows, phase coupling is an important topic. In this case, the flow can either be, one-way coupled or two-way coupled. One-way coupling is if the movement of the particles is affected by the continuous phase, but the continuous phase is not affected by the particles. On the other hand, the two-way coupling is when the effect mutual between the flows. Figure 3.10 and 3.11, is an illustration of one-way coupling and two-way coupling.

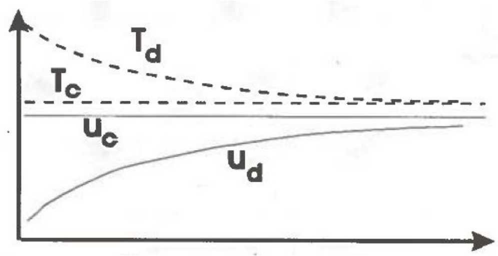

Figure 3.10: Illustration of one-way coupling Multiphase-flows [17]

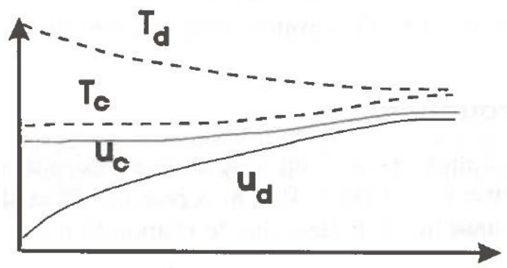

Figure 3.11: Illustration of two-way coupling Multiphase-flows[17]

T_d and T_c is the temperature of the discrete phase and continuous phase. u_d and u_c is the velocity of the discrete phase and continuous phase. Since this case operating in a dilute flow, it is assumed that this is one-way coupled.

Stokes Number

Stokes number is an important dimensionless parameter, describing the ability of the particles to follow the flow. Stokes number is defined by the ratio of the characteristic time of a particle and the characteristic time of the flow:

$$St = \frac{\tau_V}{\tau_F} \tag{3.14}$$

Calculation of the Stokes number is placed in appendix 6.3. If St<<1 the particles response time is small and the particles are able to follow the surrounding flow. If St>>1 the fluid flow will affect the particle only a bit [17]. From the calculation is can be seen that particles around 1000 μm, have a Stokes number about 1, and therefore, these particles can have difficulties of being carried of the continuous phase.

Particle Forces

This case is operating at steady state, and the particles are spherical. Since this case is gas-particle flow with small density ratio, at steady state condition, some forces can be neglected. Forces that need to be taken into consideration is the steady-state drag, lift force, and the gravitational force. Calculations of the forces are in appendix [?]

Steady-State drag force

The steady-state drag force acting on the particle, when there is no acceleration in the relative velocity between the particle and the continuous phase. The drag force is presented in equation 3.15:

$$F_D = 1/2\rho C_D A(u - v)|u - v| \tag{3.15}$$

Where C_D is the drag coefficient, and A is the area of the particle.

Gravitational force

The gravitational force is a natural phenomenon and for the particle is presented by:

$$F_g = m_p g \tag{3.16}$$

The mass of the particle is calculated by the density and the volume of the particle:

$$m_p = \rho_p \frac{4}{3}\pi r^3 \tag{3.17}$$

Saffman Lift Force

The saffman lift force accounts for the pressure distribution on the particle due to particle rotation [17]. The pressure distribution is caused by a difference in velocity under and above the particle, as illustrated in figure 3.12.

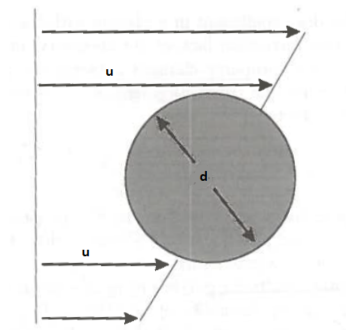

Figure 3.12: Illustration of the lift force effect [17]

The Saffman equation is stated as:

$$F_L = 1.61\mu_p d_p |u - v| \sqrt{Re_G} \tag{3.18}$$

The shear Reynolds number (Re_G) is based on the shear velocity and is calculated by:

$$Re_G = \frac{\rho V_{shear} d_p}{\mu_p} \tag{3.19}$$

The shear velocity is the ratio of the shear stress at the pipe wall and the fluid density, squared [18]

$$V_{shear} = \sqrt{\frac{(\rho_p - \rho_c) g d_p}{6\rho_c}} \tag{3.20}$$

3.5.2 Rosin-Rammler Distribution

In sprays, different sizes of droplets are caused. Some are small, and some are big and is describes by a size range where the particle sizes are within. The particle distribution is typically described by a histogram, where a frequency shows each particle size in the dataset.

Rosin-Rammler is often used in spray flows to represent the droplet size distribution. Rosin-rammler is expressed by:

$$Q = 1 - exp\left(-\frac{D}{X}\right)^q \tag{3.21}$$

Where:

- Q = the fraction of the total volume contained in droplets of diameter less than D.

- D = diameter

X and q are constants which describing the drop size distribution in sprays. q is the spread parameter of the droplet size. Typical the value of q is between 1,5-4, and the higher the value is, the more uniform is the spray.

X can be determined from the mass median diameter and q:

$$X = \frac{D_{mM}}{0,693^{1/q}} \tag{3.22}$$

Particle Distribution

Rosin-rammler (RR) distribution is used in the simulation to simulate the range of different particle diameters. It was not possible to obtain specification about particle distribution on a nozzle from the nozzle manufacturers. Therefore, other cases with atomizing nozzles have been used for the investigation.

A study of spray cooling had information about particle distribution for a nozzle. Therefore, the specifications for that nozzle is used in the first case of simulations [19].
When setting up the RR distribution, properties for the particles sizes for the injection is necessary. These parameters are the minimum, maximum, and mean diameters of the particles, which can be read on figure 3.13. Another important parameter is the spread parameter, the spread parameter can be read from the slope of a RR-plot.

Therefore, a RR-plot needs to be created to get the spread parameter. This is done from the particle distribution. The particle distribution of the study is illustrated in figure 3.13

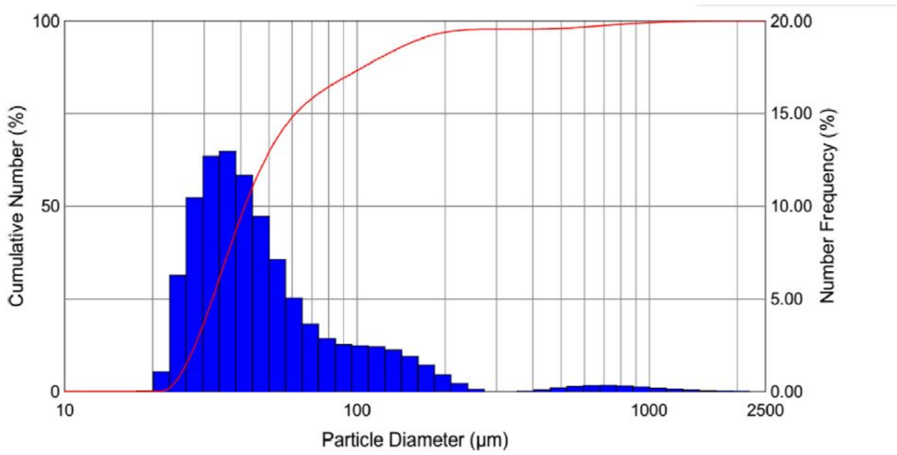

Figure 3.13: Particle distribution spray cooling nozzle [19]

From the plot it is possible to retrieve information to make the rosin-rammler plot of the particle distribution:

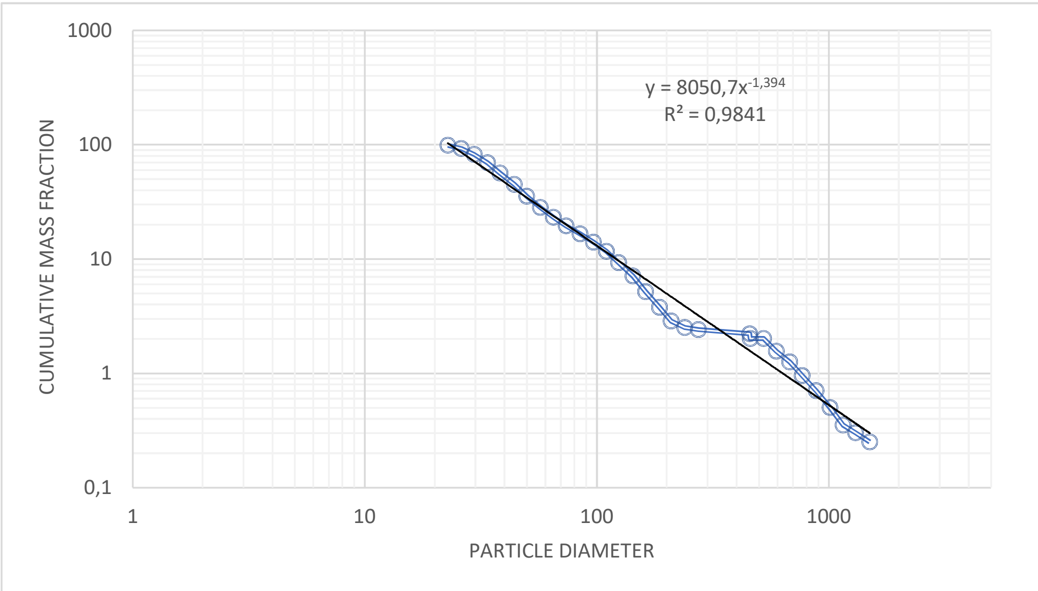

Figure 3.14: Rosin-rammler plot of the particle distribution

The slope of the graph is the spread parameter (1.394) of the particle distribution of the spray cooling study. This spread parameter is used in the simulations for this study.

3.5.3 Discrete Phase Model

The discrete phase model (DPM) is used for the particle trajectory. The model is based on Euler Lagrange approach, and the continuous phase is solved by the Navier-stokes equations, as described earlier. While the dispersed phase is solved by tracking a certain amount of particles, through the continuous flow field.

Turbulent Dispersion

Due to the turbulence in the continuous phase, Ansys fluent account for this by using stochastic tracking. The stochastic tracking is also known as random walk, because of the inclusion of the effect from the instantaneous turbulent velocity fluctuations on the particle trajectories. The trajectory equation is listed as:

$$u = \bar{u} + u' \tag{3.23}$$

Stochastic tracking is based on the mean fluid phase velocity ($\bar{u}$). By integrating the trajectory equations for each individual particle, Ansys Fluent predicts the turbulent dispersion.

3.5.4 Simulations

Through the study, a set of simulations will be necessary. This study will contain simulation of the two geometries at three different velocities, and with two different injection forms. Therefore, some considerations are made to minimize the number of simulations.
First a set of simulations is done for the straight pipe, and is listed in table 3.2:

Table 3.2: Table of the injection form simulations

Injection form simulations	
With the flow	Against the flow
10 m/s	10 m/s
20 m/s	20 m/s
40 m/s	40 m/s

The first set of simulations are of the two different injection forms, which is injection with the flow, and injection against the flow. As illustrated in figure 3.15 and 3.16.

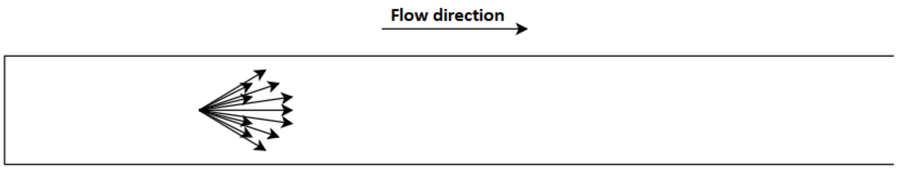

Figure 3.15: Injection with the flow

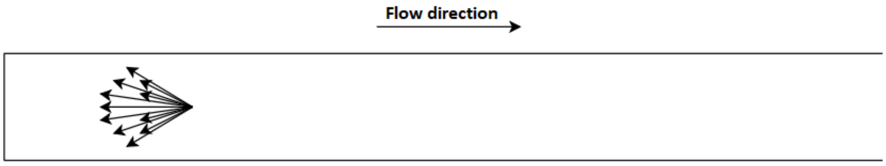

Figure 3.16: Injection against the flow

Results from the injection form is presented in section 3.6. The results showed that there was not a significant difference in the injection with or against the flow direction. Therefore, the injection for further simulations is with the flow.

As showed in figure 3.1 and 3.2, two different geometries is investigated. The two different geometries are studied at different flow velocities. Table 3.3 is a table of the performed simulations.

Table 3.3: Table of the pipe geometries simulations

Pipe geometries simulations	
Straight Pipe	U-form Pipe
10 m/s	10 m/s
20 m/s	20 m/s
40 m/s	40 m/s

3.5.5 Used Parameters

To give an overview of the settings and properties used in the simulation, some tables of the important parameters in the simulation are listed.

Table 3.4 is a table of the parameters used to the simulation.

Table 3.4: Table of the used parameters for the simulation

Simulation setup	
Turbulence model	k-ϵ, Standard wall function
Solution method	Simple
Discretization scheme	First and Second order
Solver	Incompressible, steady-state
Discrete Phase	Interaction With Continuous Phase Solid cone Injection
Turbulent Dispersion	Discrete Random Walk Model

Table 3.5 is a table of the properties to set up the injection in the DPM model.

Table 3.5: Table of the injection properties

Injection properties	
Velocity	1.243 m/s
Cone angle	70°
Nozzle orifice	0.16 cm
Flow rate	0.003 kg/s
Min. Diameter	0.002 cm
Max. Diameter	0.15 cm
Mean Diameter	0.0042
Spread Parameter	1.394
Number of Diameters	20

The properties for the nozzle are from the study of the spray cooling, as mentioned previously.

3.6 Results

In this section, the results of the simulation will be presented and explained. The section is divided into subsections to make manageable. First, the results for the injection direction is presented, then the results from the U-pipe geometry is presented.

In figure 3.17, planes where the particles are sampled, are illustrated. The results are sampled right after the injection and then at the outlet, to see which size of particle that survives.

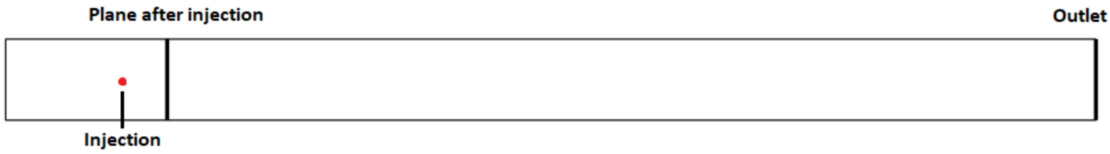

Figure 3.17: Illustration of the sample planes on the geometry

3.6.1 Results - Injection form

The results from the injection form are the first set of results to be represented. The injection form is to see if the direction of the injection has an impact on the survival of the particles. The results are from the injection forms illustrated in figure 3.15 and 3.16.

The particle distribution for the injection is the same for every injection. In figure 3.18 the particle distribution for the simulations is illustrated.

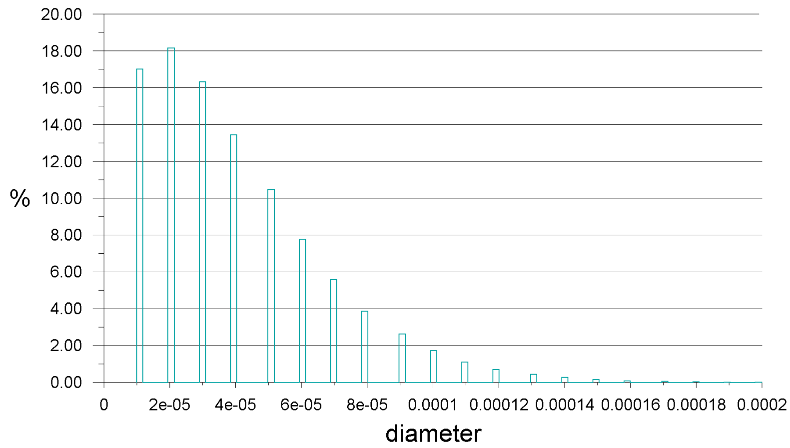

Figure 3.18

Different velocities are used for the simulation. Therefore, the results are divided into subsection for differentiation. Histograms presented to the left are of injection with the flow direction, and histograms to the right are of injection opposite the flow direction.

Velocity - 10 m/s

The particle distribution of the simulation with a continuous phase velocity at 10 m/s is illustrated in figure 3.19 and 3.20.

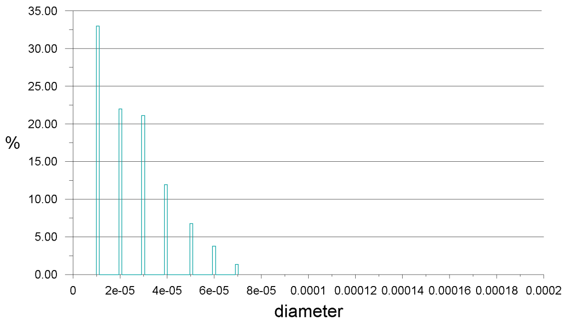

Figure 3.19: Histogram of the particles at the injection

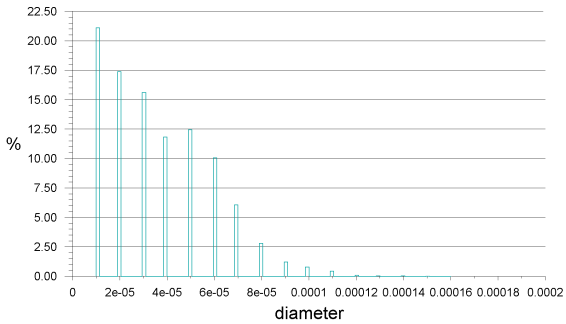

Figure 3.20: Histogram of the particles at the outlet

Figure 3.19 and 3.20 illustrates the particles that survived. From the injection with the direction particle up to 70 μm survives, where with the injection in the opposite direction particles up to 140 μm survives.

Velocity - 20 m/s

The particle distribution of the simulation with a continuous phase velocity at 20 m/s is illustrated in figure 3.21 and 3.22.

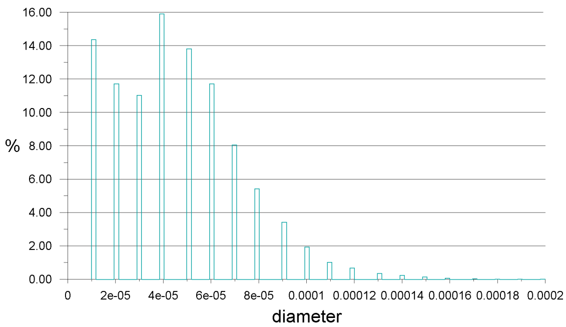

Figure 3.21: Histogram of the particles at the injection

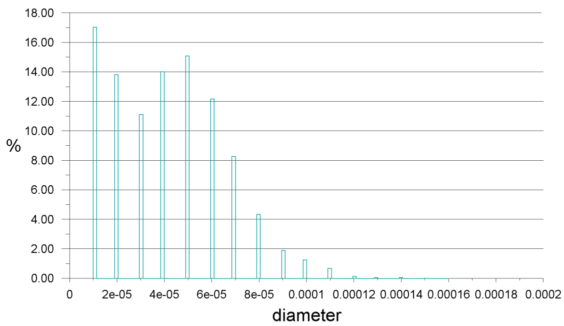

Figure 3.22: Histogram of the particles at the outlet

With the injection of 20 m/s, the particle distribution of the two injection form is quite similar. At the injection with the continuous phase, a bit bigger particles survive.

Velocity - 40 m/s

The particle distribution of the simulation with a continuous phase velocity at 40 m/s is illustrated in figure 3.23 and 3.24.

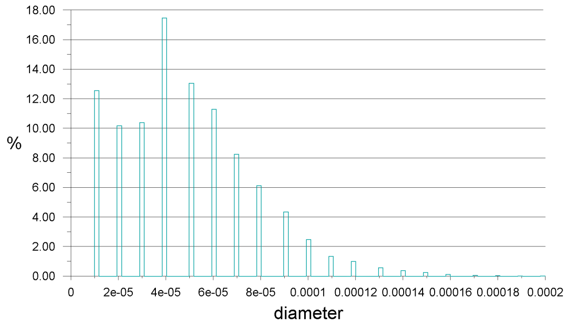

Figure 3.23: Histogram of the particles at the injection

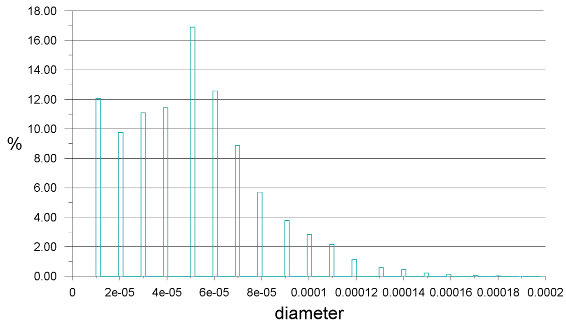

Figure 3.24: Histogram of the particles at the outlet

From the injection at 40 m/s, there is not a significant difference in the particle distributions.

By looking at the histograms of the particle distribution, it shows that there was not a significant difference in the injection with the flow or opposite the flow. Therefore, the injection form with the flow is used for further simulations.

Particle trajectory

Particle trajectories at each velocity are represented in figure 3.25, 3.26 and 3.27. The figure gives a good view of the particle diameters down through the pipe and the survival of the big particles.

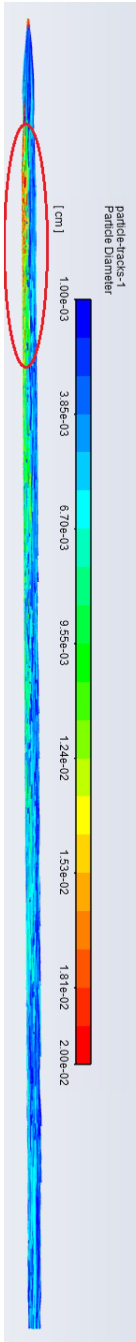

Figure 3.25: Illustration of the particle trajectory at 10 m/s

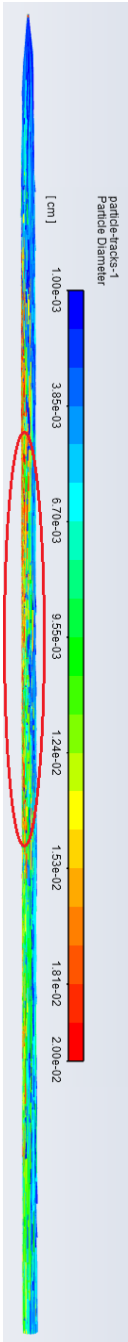

Figure 3.26: Illustration of the particle trajectory at 20 m/s

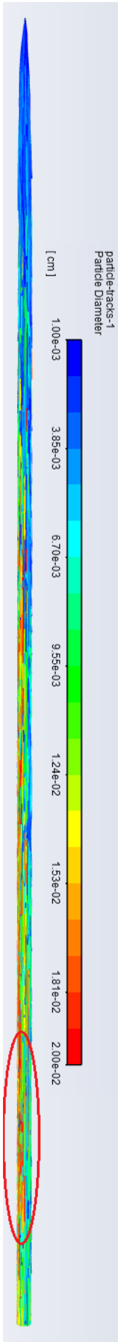

Figure 3.27: Illustration of the particle trajectory at 40 m/s

The trajectories are of 2000 particles, and the higher velocity, the more particles survive. The biggest particles are with the color red, and by looking at the figures, it is clear that at a higher velocity, the biggest particles survive longer (market with a red circle).

3.6.2 Results - U-pipe

Another thing stated in the project definition is to see the impact on the particle survival by a change in the geometry. Here the results from the U-pipe is presented.

10 m/s

Figure 3.28 is the particles that survive through the geometry.

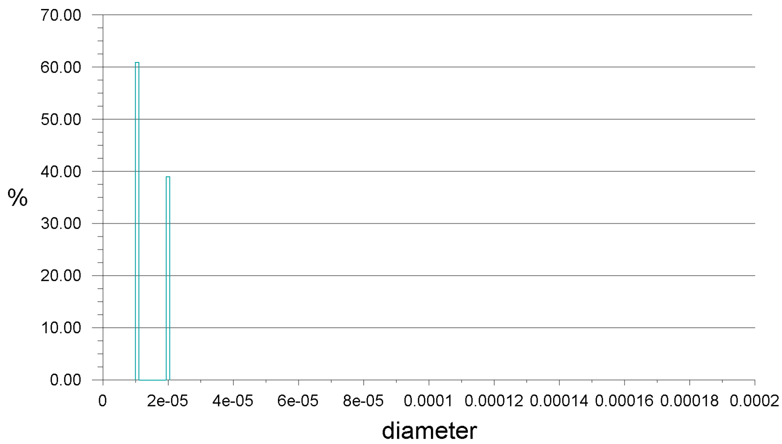

Figure 3.28: Particle distribution for the u-pipe at 10 m/s

Many of the particles have been trapped through the pipe, but 8 particles survived. And the particles are with a diameter of 20 μm and 10 μm.

20 m/s

Figure 3.29 is the particles that survive with an increase in the gas phase velocity.

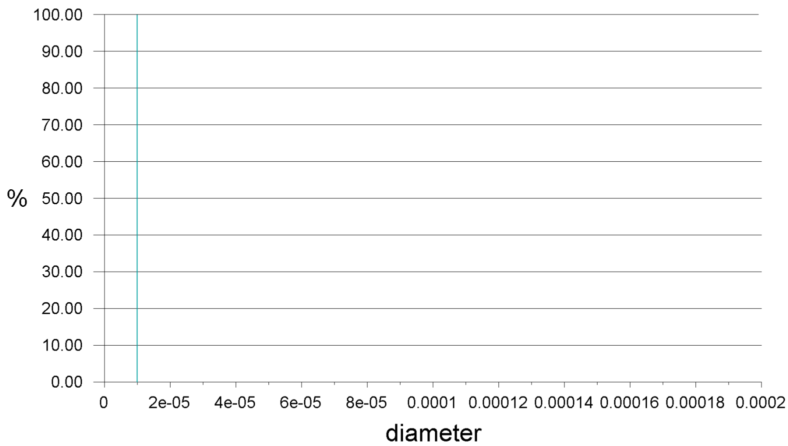

Figure 3.29: Particle distribution for the u-pipe at 20 m/s

Only 6 particles survived, and these particles have a diameter of 10 μm.

40 m/s

The last histogram is with a gas phase velocity of 40 m/s

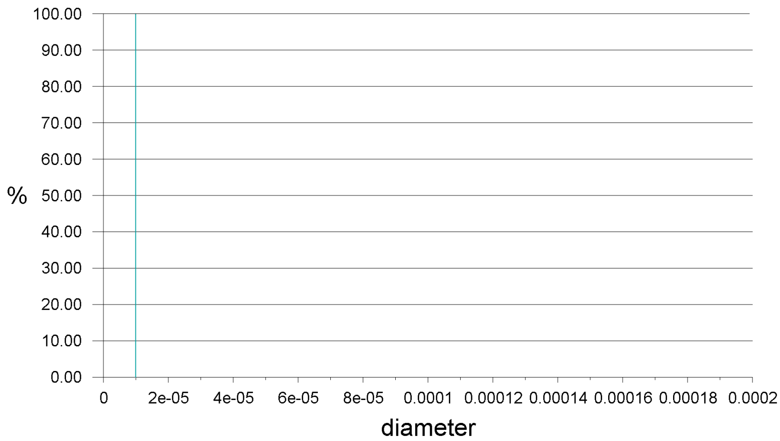

Figure 3.30: Particle distribution for the u-pipe at 40 m/s

Again a small number of particles survived, in this case only 2 survived.

Particle Trajectory

Particle trajectories from the U-pipe is illustrated in figure 3.28, 3.29 and 3.30. The trajectories gives a vision of where the particles are trapped.

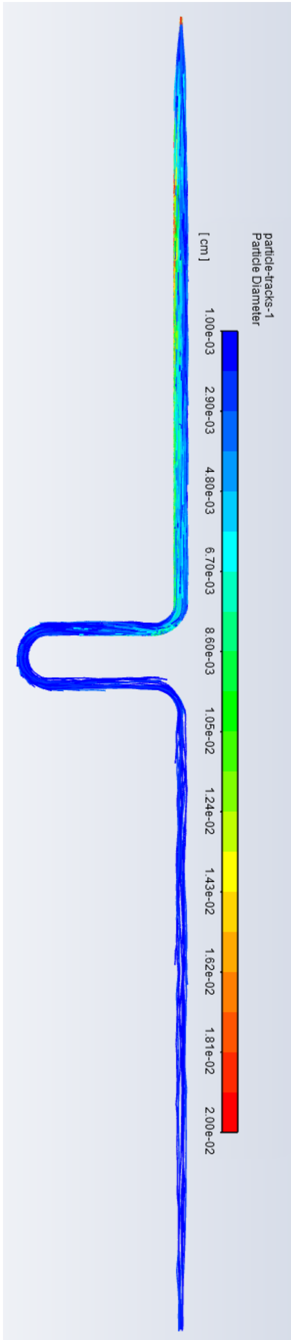

Figure 3.31: Illustration of the particle trajectory at 10 m/s

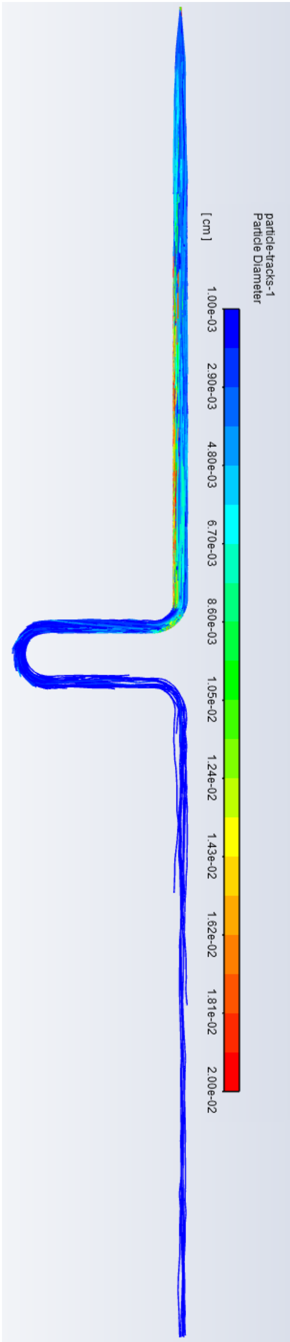

Figure 3.32: Illustration of the particle trajectory at 20 m/s

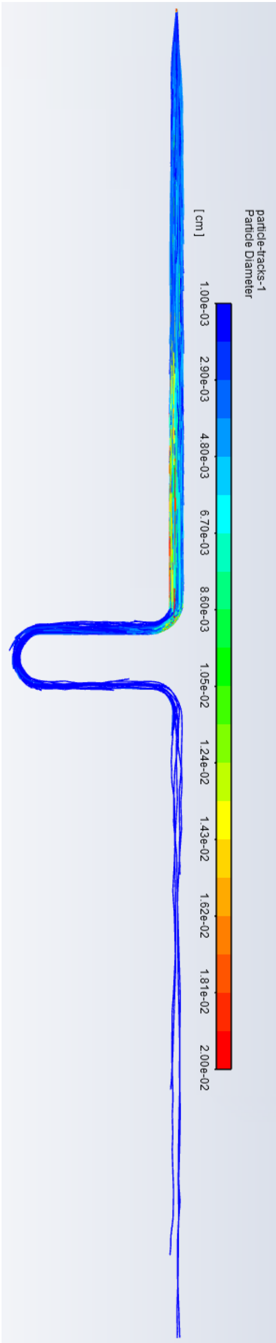

Figure 3.33: Illustration of the particle trajectory at 40 m/s

3.6.3 Residual plot

Trough the simulations the residual plot is used to check for convergence. A residual plot is illustrated in figure 3.34. The residual plot shows the error in the system, and when the error does not change any more, the simulation is seen as converged.

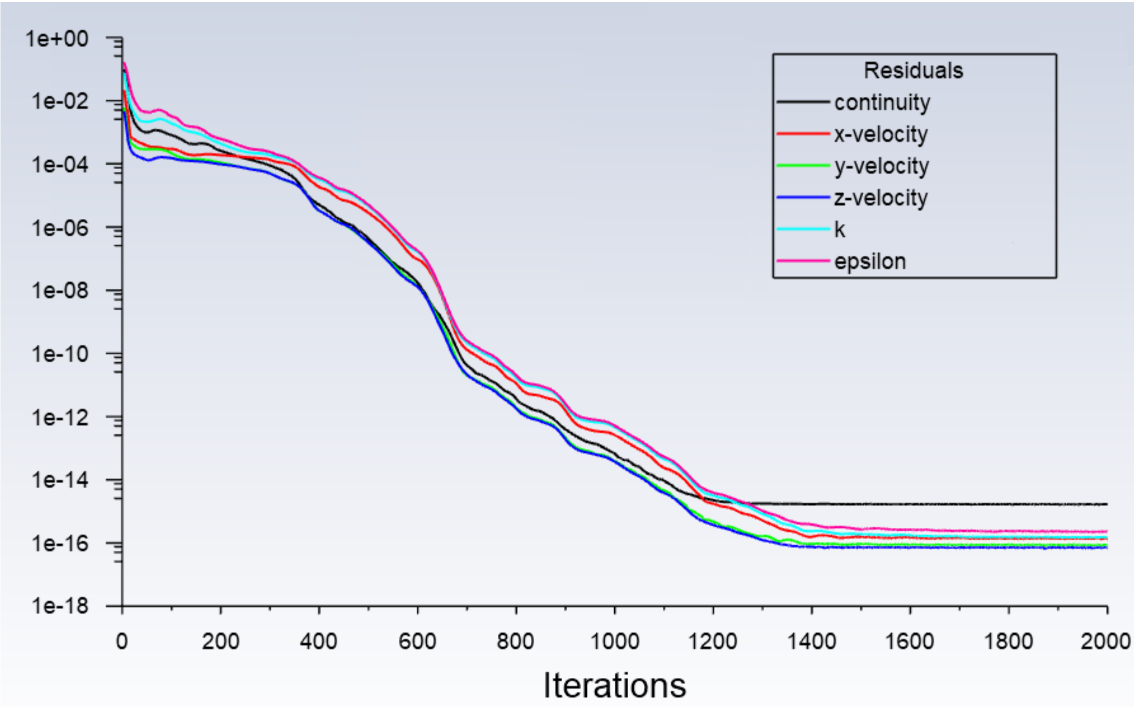

Figure 3.34: Illustration of a residual plot

Chapter 4

Discussion

There is excessive use of scavenger because the quill is used as injection form. The quill pours the scavenger into the pipeline, and therefore it is presumed that the particles are too big and the majority falls to the bottom and is useless.
The purpose of this project was primarily to investigate the H_2S injection by a nozzle. It is assumed that a nozzle is better than the quill, because of the smaller particles which are able to be carried of the continuous phase. The scavenger requires 15-20 seconds to react with the H_2S. Therefore the survival of the particles is essential of good efficiency in H_2S removal.
The project did not turn out as planned. The purpose was to investigate different nozzles with different particle distributions. But the nozzle manufacturers would not give specific information about the nozzles, and therefore the particle distribution should be found in another way. A previous study of spray cooling was found, and the specifications of their nozzle were used for this injection. Since the specifications of the nozzles are very difficult to achieve, only one nozzle was investigated in this project.

A lot of previous work on the H_2S scavenger injection has been made, these studies are reviewed to make sure that this study differs from their investigations. The previous studies had a focus on the optimum design of the injection, the optimum dose rate, and different scavengers. To differentiate from these, this project focused on the survival of the particles due to the nozzle injection and geometry design. Another thing that is investigated is the injection direction.

One of the topics for this project was a CFD simulation of the injection. The pre-processing part did not cause any significant problems. The meshing part and quality part went straight forward. But the grid independence study showed that a significantly smaller amount of cells was enough for the simulation, and therefore the mesh resolution had to be changed.
The simulation in Fluent was a bit more challenging to set up. The primary part of the simulation was the DPM model, which required a lot of adjustment. First of all, the type of injection had to be chosen, and all the different injection types had

various adjustments. But after trial and error with the different types, the solid cone injection was the ideal one for this simulation. The particles distribution had to be set up in the DPM model, and this was done by the rosin-rammler distribution. But there were some troubles with the particle distribution when simulating. It turned out that the spread between the smallest and the biggest particle was too big, and Fluent could not handle this. Therefore, adjustments in the particle distribution had to be done to get some usable results.

The project definition stated several questions, one of them was the injection direction. The injection in the opposite direction than the continuous flow showed that at low flow velocity, more particles survived, but at high flow velocity, the injection with the flow was a bit better. Taken into consideration that the scavenger would be trapped on the nozzle, the injection in the opposite direction is not the optimum injection form. Therefore, the injection with the continuous flow direction is used for the other simulations. Generally, the two injection direction was similar in the particle distribution at the outlet.
Another thing stated was the design in the geometry. Two designs of pipes were created: A straight pipe and a pipe with a u-bend. The straight pipe showed that a significant amount of particles survived through the pipe. While the u-bend design showed that only a few particles survived and all other particles was trapped on the walls. Most particles survived at low flow velocity, therefore when at a change in the pipe system, the flow velocity should be lowered.

Assumed that the quill pours a system with large particles, and many of these falls to the bottom, the small particles would be more ideal for H_2S scavenger injection. The results from the nozzle showed that the big particles were trapped at the walls, while the smaller particles survived to the outlet, and had sufficient time to react with the H_2S.

Further study of this project would be, to test a nozzle with a smaller particles distribution, to get an ideal nozzle with a lot of survived particles. Furthermore, a reaction between the scavenger and the H_2S is ideal to set up in fluent and then see the reaction time, between the scavenger and the H_2S, for the ideal nozzle.

Chapter 5

Conclusion

The purpose of this project was to investigate the survival of the particles by a nozzle atomizing injection. The simulations of the nozzle went very well and gave some useful results. The results showed that the large particles ($>100\mu m$) falls to the bottom of the pipe, while the small particles ($<100\mu m$) survives through the pipe. Therefore, a nozzle with a small particle distribution could be the optimum injection for the scavenging process.

Furthermore, it was investigated whether a change in the geometry design affected the survival of the particles. The results from the u-pipe showed that only a significantly small amount of particles survived, and the rest was trapped at the walls at the bend. Therefore, when changing the pipe direction, a decrease in the flow velocity would be optimum.

Bibliography

[1] M.G. Lioliou, C.B. Jenssen, K. Øvsthus, A-M. Bruräs, and Ø.L. Aasen. Design principles for h2s scavenger injection systems. *Oilfield Chemistry Symposium*, March 2018.

[2] Anders Andreasen. Personal cummunication. Date: 29-01-2019 - Rambøll.

[3] GateKeeper. H2s scavenging: Using triazine. GateKeeper homepage. https://www.gateinc.com/gatekeeper/gat2004-gkp-2014-05.

[4] Kofle. Static inline mixer. Koflo homepage. https://www.koflo.com/static-mixers.html.

[5] United states department of labor. Health hazards. Osha homepage. https://www.osha.gov/SLTC/hydrogensulfide/hazards.html.

[6] Health and Safety executive. Managing hydrogen sulfide detection offshore.

[7] Erik Jorgensen. Personal cummunication. ConocoPhilips.

[8] GateKeeper. H2s scavenging: Using triazine. GateKeeper homepage. https://www.gateinc.com/gatekeeper/gat2004-gkp-2014-04.

[9] Trimeric. Design of direct injection h2s scavenging systems. Trimeric homepage. http://www.trimeric.com/assets/design-of-direct-injection-h2s-scavenging-systems.pdf.

[10] T.M. Elshiekh, S.A. Khalil, A.M. Alsabagh, and H.A. Elmawgoudu. Simulation for estimation of hydrogen sulfide scavenger injection dose rate for treatment of crude oil. *Eqyptian Journal of Petroleum*, December 2015.

[11] T.M. Elshiekh, S.A. Khalil, A.M. Alsabagh, and H.A. Elmawgoud. Optimum injection dose rate of hydrogen sulfide scavenger for treatment of petroleum crude oil. *Eqyptian Journal of Petroleum*, March 2016.

[12] T.M. Elshiekh, S.A. Khalil, A.M. Alsabagh, H.A. Elmawgoudu, and M. Tawfik. Modeling of hydrogen sulfide removal from ptroleum production facilities using h2s scavenger. *Eqyptian Journal of Petroleum*, June 2015.

[13] Natália A. Portela, Samantha R.C. Silva, Luciana F.R. de Jesus, Guilherme P. Dalmaschio, Cristina M.S. Sad, Eustáquio V.R. Castro, Milton K. Morigaki,

Eloi A. Silva Filho, and Paulo R. Filgueiras. Spectroscopic evaluation of commercial h2s scavengers. *Fuel*, 2018.

[14] Nadia G. Kandile, Taha M.A. Razek, Ahmed M. Al-Sabagh, and Maamoun M.T. Khattab. Synthesis and evaluation of some amine compounds having surface active properties as h2s scavenger. *Egyptian Journal of Petroleum*, 2014.

[15] H. K Versteeg and W. Malalasekera. *Computational fluid dynamics*. Pearson, second edition, 2007.

[16] Sandia National Laboratories. Cubit software. Cubit sandia homepage. https://cubit.sandia.gov/.

[17] C. Crowe, M. Sommerfeld, and Y. Tsuji. *Multiphase flows with droplets and particles*. CRC Press, 1998.

[18] K. C Wilson, G. R Addie, A. Sellgren, and R. Clift. *Slurry Transport Using Centrifugal Pumps*. Springer, third edition, 2006.

[19] X. Liu, R. Xue, Y. Ruan, L. Chen, X. Zhang, and Y. Hou. Effect of injection pressure difference on droplet size distribution and spray cone angle in spray cooling of liquid nitrogen. *Cryogenics*, February 2017.

Chapter 6

Appendix

6.1 Time Ratio

Momentum response time

The momentum response time is defined as, the time a particle required to respond to a change in velocity. The momentum response time equation:

$$T_V = \frac{\rho_d D^2}{18\mu} \tag{6.1}$$

Where:

- ρ_d = Density of dispersed phase
- D = Diameter of the particle
- μ = Is the viscosity of the ....

Particle collision time

The average time between particle-particle collisions is defined from the collision frequency:

$$f_c = n\pi D^2 v_r \tag{6.2}$$

Where:

- n = Number density of particles
- v_r = Particle velocity

The time between collisions equals:

$$T_C = \frac{1}{f_c} = \frac{1}{n\pi D^2 v_r} \tag{6.3}$$

Time Ratio

Then the time ratio can be expressed as:

$$\frac{T_V}{T_C} = \frac{n\pi\rho_d D^4 v_r}{18\mu} \tag{6.4}$$

Since the bulk density $\bar{\rho}_d$ is equal to, the number of density and the mass of an individual particle. Equation 6.4 can be written as [17]:

$$\frac{T_V}{T_C} = \frac{\bar{\rho}_d D v_r}{3\mu} \tag{6.5}$$

6.2 Particle Loading

Particle Loading

$\rho_c := 11.8 \ \frac{kg}{m^3}$ $\quad u := 10 \ \frac{m}{s}$ $\quad \rho_d := 1200 \ \frac{kg}{m^3}$

$Z = \frac{M_{flow.d}}{M_{flow.c}}$ $\quad A_{pipe} := \frac{\pi}{4} \cdot (10 \ cm)^2 = 78.54 \ cm^2$

$V_{flow} := A_{pipe} \cdot u = 0.079 \ \frac{m^3}{s}$

$M_{flow.c} := \rho_c \cdot V_{flow} = 0.927 \ \frac{kg}{s}$

$M_{flow.d} := 0.003 \ \frac{kg}{s}$ From the injection properties

$Z := \frac{M_{flow.d}}{M_{flow.c}} = 0.00324$

6.3 Stokes Number

Stokes number - 10 m/s:

$\rho_p := 1200 \ \frac{kg}{m^3}$ $\rho_c := 11.8 \ \frac{kg}{m^3}$ $\mu_p := 0.00634 \ \frac{kg}{m \cdot s}$ $d_p := \begin{bmatrix} 20 \ \mu m \\ 40 \ \mu m \\ 100 \ \mu m \\ 200 \ \mu m \\ 500 \ \mu m \\ 1000 \ \mu m \\ 1500 \ \mu m \\ 2000 \ \mu m \end{bmatrix}$

$$\tau_V := \frac{\left(\rho_p - \rho_c\right) \cdot {d_p}^2}{18 \cdot \mu_p} = \begin{bmatrix} 4.165 \cdot 10^{-6} \\ 1.666 \cdot 10^{-5} \\ 1.041 \cdot 10^{-4} \\ 4.165 \cdot 10^{-4} \\ 0.003 \\ 0.01 \\ 0.023 \\ 0.042 \end{bmatrix} s$$

$d := 10 \ cm$ Diameter of the pipe

$u := 10 \ \frac{m}{s}$ Gas stream velocity

$$\tau_F := \frac{d}{u} = 0.01 \ s$$

$$St := \frac{\tau_V}{\tau_F} = \begin{bmatrix} 4.165 \cdot 10^{-4} \\ 0.002 \\ 0.01 \\ 0.042 \\ 0.26 \\ 1.041 \\ 2.343 \\ 4.165 \end{bmatrix} \qquad \begin{bmatrix} 20 \ \mu m \\ 40 \ \mu m \\ 100 \ \mu m \\ 200 \ \mu m \\ 500 \ \mu m \\ 1000 \ \mu m \\ 1500 \ \mu m \\ 2000 \ \mu m \end{bmatrix}$$

Stokes number 20 m/s:

$\rho_p := 1200 \frac{kg}{m^3}$ $\rho_c := 11.8 \frac{kg}{m^3}$ $\mu_p := 0.00634 \frac{kg}{m \cdot s}$ $d_p := \begin{bmatrix} 20\ \mu m \\ 40\ \mu m \\ 100\ \mu m \\ 200\ \mu m \\ 500\ \mu m \\ 1000\ \mu m \\ 1500\ \mu m \\ 2000\ \mu m \end{bmatrix}$

$$\tau_V := \frac{(\rho_p - \rho_c) \cdot {d_p}^2}{18 \cdot \mu_p} = \begin{bmatrix} 4.165 \cdot 10^{-6} \\ 1.666 \cdot 10^{-5} \\ 1.041 \cdot 10^{-4} \\ 4.165 \cdot 10^{-4} \\ 0.003 \\ 0.01 \\ 0.023 \\ 0.042 \end{bmatrix} s$$

$d := 10\ cm$ Diameter of the pipe

$u := 20 \frac{m}{s}$ Gas stream velocity

$$\tau_F := \frac{d}{u} = 0.005\ s$$

$$St := \frac{\tau_V}{\tau_F} = \begin{bmatrix} 8.329 \cdot 10^{-4} \\ 0.003 \\ 0.021 \\ 0.083 \\ 0.521 \\ 2.082 \\ 4.685 \\ 8.329 \end{bmatrix} \quad \begin{bmatrix} 20\ \mu m \\ 40\ \mu m \\ 100\ \mu m \\ 200\ \mu m \\ 500\ \mu m \\ 1000\ \mu m \\ 1500\ \mu m \\ 2000\ \mu m \end{bmatrix}$$

Stokes number 40 m/s:

$\rho_p := 1200 \frac{kg}{m^3}$ $\rho_c := 11.8 \frac{kg}{m^3}$ $\mu_p := 0.00634 \frac{kg}{m \cdot s}$ $d_p := \begin{bmatrix} 20\ \mu m \\ 40\ \mu m \\ 100\ \mu m \\ 200\ \mu m \\ 500\ \mu m \\ 1000\ \mu m \\ 1500\ \mu m \\ 2000\ \mu m \end{bmatrix}$

$$\tau_V := \frac{(\rho_p - \rho_c) \cdot {d_p}^2}{18 \cdot \mu_p} = \begin{bmatrix} 4.165 \cdot 10^{-6} \\ 1.666 \cdot 10^{-5} \\ 1.041 \cdot 10^{-4} \\ 4.165 \cdot 10^{-4} \\ 0.003 \\ 0.01 \\ 0.023 \\ 0.042 \end{bmatrix} s$$

$d := 10\ cm$ Diameter of the pipe

$u := 40 \frac{m}{s}$ Gas stream velocity

$$\tau_F := \frac{d}{u} = 0.003\ s$$

$$St := \frac{\tau_V}{\tau_F} = \begin{bmatrix} 0.002 \\ 0.007 \\ 0.042 \\ 0.167 \\ 1.041 \\ 4.165 \\ 9.371 \\ 16.659 \end{bmatrix} \qquad \begin{bmatrix} 20\ \mu m \\ 40\ \mu m \\ 100\ \mu m \\ 200\ \mu m \\ 500\ \mu m \\ 1000\ \mu m \\ 1500\ \mu m \\ 2000\ \mu m \end{bmatrix}$$

6.4 Particle Forces

Particle Forces

$u := 10\ \frac{m}{s}$ $\quad v := 1.234\ \frac{m}{s}$ $\quad \rho_c := 11.8\ \frac{kg}{m^3}$ $\quad \rho_p := 1200\ \frac{kg}{m^3}$

$d_p := 42\ \mu m$ $\quad \mu_p := 0.00634\ \frac{kg}{m \cdot s}$ $\quad A := \frac{\pi}{4} \cdot 42\ \mu m^2 = \left(3.299 \cdot 10^{-11}\right)\ m^2$

Forces - 10 m/s

Drag

$$Re := \frac{\rho_c \cdot u \cdot d_p}{\mu_p} = 0.782$$

$$C_D := \frac{24}{Re} = 30.702$$

$$F_D := \frac{1}{2} \cdot \rho_c \cdot C_D \cdot A \cdot (u - v) \cdot |u - v| = \left(4.592 \cdot 10^{-7}\right)\ N$$

Gravitational Force

$$m_p := \rho_p \cdot \left(\frac{4}{3} \cdot \pi \cdot \left(\frac{d_p}{2}\right)^3\right) = \left(4.655 \cdot 10^{-8}\right)\ gm$$

$$F_g := m_p \cdot g = \left(4.565 \cdot 10^{-10}\right)\ N$$

Liftforce

$$V_{shear} := \sqrt{\frac{\left(\rho_p - \rho_c\right) \cdot g \cdot d_p}{6 \cdot \rho_c}} = 0.083\ \frac{m}{s}$$

$$Re_G := \frac{\rho_p \cdot V_{shear} \cdot d_p}{\mu_p} = 0.661$$

$$F_{lift} := 1.61 \cdot \mu_p \cdot d_p \cdot |u - v| \cdot \sqrt{Re_G} = \left(3.055 \cdot 10^{-6}\right)\ N$$

Forces - 20 m/s $u := 20 \ \frac{m}{s}$

Drag

$$Re := \frac{\rho_c \cdot u \cdot d_p}{\mu_p} = 1.563$$

$$C_D := \frac{24}{Re} = 15.351$$

$$F_D := \frac{1}{2} \cdot \rho_c \cdot C_D \cdot A \cdot (u - v) \cdot |u - v| = \left(1.052 \cdot 10^{-6}\right) \ N$$

Gravitational Force

$$m_p := \rho_p \cdot \frac{4}{3} \cdot \pi \cdot \left(\frac{d_p}{2}\right)^3 = \left(4.655 \cdot 10^{-8}\right) \ gm$$

$$F_g := m_p \cdot g = \left(4.565 \cdot 10^{-10}\right) \ N$$

Liftforce

$$V_{shear} := \sqrt{\frac{\left(\rho_p - \rho_c\right) \cdot g \cdot d_p}{6 \cdot \rho_c}} = 0.083 \ \frac{m}{s}$$

$$Re_G := \frac{\rho_p \cdot V_{shear} \cdot d_p}{\mu_p} = 0.661$$

$$F_{lift} := 1.61 \cdot \mu_p \cdot d_p \cdot |u - v| \cdot \sqrt{Re_G} = \left(6.541 \cdot 10^{-6}\right) \ N$$

Forces - 40 m/s $u := 40\ \frac{m}{s}$

Drag

$$Re := \frac{\rho_c \cdot u \cdot d_p}{\mu_p} = 3.127$$

$$C_D := \frac{24}{Re} = 7.676$$

$$F_D := \frac{1}{2} \cdot \rho_c \cdot C_D \cdot A \cdot (u - v) \cdot |u - v| = \left(2.245 \cdot 10^{-6}\right)\ N$$

Gravitational Force

$$m_p := \rho_p \cdot \frac{4}{3} \cdot \pi \cdot \left(\frac{d_p}{2}\right)^3 = \left(4.655 \cdot 10^{-8}\right)\ gm$$

$$F_g := m_p \cdot g = \left(4.565 \cdot 10^{-10}\right)\ N$$

Liftforce

$$V_{shear} := \sqrt{\frac{\left(\rho_p - \rho_c\right) \cdot g \cdot d_p}{6 \cdot \rho_c}} = 0.083\ \frac{m}{s}$$

$$Re_G := \frac{\rho_p \cdot V_{shear} \cdot d_p}{\mu_p} = 0.661$$

$$F_{lift} := 1.61 \cdot \mu_p \cdot d_p \cdot |u - v| \cdot \sqrt{Re_G} = \left(1.351 \cdot 10^{-5}\right)\ N$$